

On the Impact of Mutual Coupling on RIS-Assisted Channel Estimation

Pinjun Zheng, *Student Member, IEEE*, Xiuxiu Ma, *Student Member, IEEE*,
and Tareq Y. Al-Naffouri, *Senior Member, IEEE*

Abstract—Amid the demand for densely integrated elements in techniques such as holographic reconfigurable intelligent surfaces (RISs), the mutual coupling effect has gained prominence. By performing a misspecified Cramér-Rao bound analysis within an electromagnetics-compliant communication model, this letter offers a quantitative evaluation of the impact of mutual coupling on RIS-assisted channel estimation. Our analysis provides insights into situations where mutual coupling can be disregarded safely. The analyses and numerical results reveal that within practical scenarios, closer integration of RIS elements or the enlargement of RIS size accentuates the impact of neglecting mutual coupling. In addition, even with mutual coupling-aware setups, excessively tight RIS element spacing can lead to substantial degradation in the channel estimation performance.

Index Terms—Reconfigurable intelligent surface, channel estimation, mutual coupling, misspecified Cramér-Rao bound

I. INTRODUCTION

Reconfigurable intelligent surface (RIS), also known as intelligent reflecting surface, empowers intelligent and programmable wireless propagation environments. To date, RIS-assisted communication, sensing, and localization in mmWave/THz band have attracted widespread attention [1]–[4]. Among the RIS-related studies, channel estimation in a RIS-assisted wireless system is a particularly essential topic since accurate channel state information is crucial for achieving optimal channel capacity [5]. Despite notable advancements in RIS-assisted channel estimation [6], [7], the oversight of practical electromagnetic attributes, such as mutual coupling among RIS unit cells, remains a critical concern.

The mutual coupling effect, which refers to the interaction between neighboring RIS unit cells, has recently gained attention in RIS-assisted communications [8]. Generally, mutual coupling among RIS unit cells can be reasonably ignored when the inter-distance is large enough (e.g., larger than half wavelength [9]). However, the emergence of techniques such as holographic multiple-input multiple-output (MIMO) necessitates ultra-dense antenna integration within a limited surface [10], rendering mutual coupling undeniable. To the best of the authors' knowledge, mutual coupling-aware channel estimation for RIS-assisted communications has not yet been studied. Given this, assessing the justifiable extent of disregarding

The authors are with the Electrical and Computer Engineering Program, Division of Computer, Electrical and Mathematical Sciences and Engineering (CEMSE), King Abdullah University of Science and Technology (KAUST), Thuwal, 23955-6900, Kingdom of Saudi Arabia. Email: {pinjun.zheng; xiuxiu.ma; tareq.alnaffouri}@kaust.edu.sa.

This publication is based upon the work supported by the King Abdullah University of Science and Technology (KAUST) Office of Sponsored Research (OSR) under Award No. ORA-CRG2021-4695.

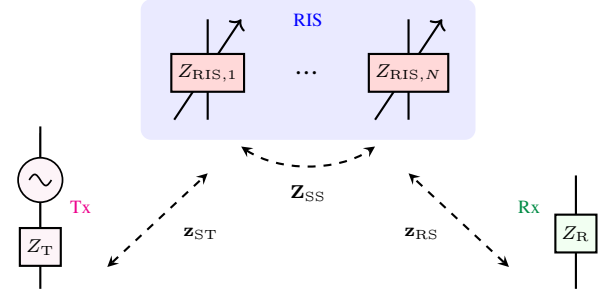


Fig. 1. Schematic illustration of the considered RIS-assisted communication system with the self and mutual coupling of RIS elements denoted as \mathbf{Z}_{SS} .

mutual coupling emerges as a key issue to be addressed. Using the misspecified Cramér-Rao bound (MCRB) [11], our results show how the system parameters like the inter-distance of RIS unit cells and the RIS size affect channel estimation performance with the mutual coupling effect and provide insights into conditions under which mutual coupling can be confidently ignored. The simulation code of this paper is available at <https://github.com/ZPinjun/Communication>.

II. SYSTEM MODEL

A. The End-to-End Electromagnetics (EM) Transfer Model

We consider an RIS-assisted single-input-single-output (SISO) communication system, where the direct path between the transmitter and the receiver is blocked. The RIS is assumed to be an array of $N_1 \times N_2$ passive yet reconfigurable scattering elements with a uniform inter-distance d . Each of these elements in turn consists of a single unit cell. To analyze the impact of mutual coupling among scattering elements of the RIS, we adopt the end-to-end EM-compliant communication model proposed in [8], which is given by

$$h_{E2E} = \mathbf{z}_{RS}^T (\mathbf{Z}_{SS} + \mathbf{Z}_{RIS})^{-1} \mathbf{z}_{ST}. \quad (1)$$

Here, $\mathbf{z}_{ST} \in \mathbb{C}^{N \times 1}$ denotes the mutual impedances between the transmitter and RIS, $\mathbf{z}_{RS} \in \mathbb{C}^{N \times 1}$ denotes the mutual impedances between the RIS and receiver, $\mathbf{Z}_{SS} \in \mathbb{C}^{N \times N}$ is a full matrix containing the self and mutual impedances among scattering elements of the RIS, and $\mathbf{Z}_{RIS} = \text{diag}\{Z_{RIS,1}, Z_{RIS,2}, \dots, Z_{RIS,N}\} \in \mathbb{C}^{N \times N}$ is a diagonal matrix containing the tunable loads $Z_{RIS,n}$ of the circuits enabling the reconfigurability of the surface, $n = 1, 2, \dots, N_1 \times N_2$. A schematic diagram of the system is provided in Fig. 1. In this model, the wireless channels correspond to the impedance vectors \mathbf{z}_{RS} and \mathbf{z}_{ST} .

Note that based on the microwave network theory [12], the commonly employed channel coefficients are essentially scattering parameters, which are equivalent characterizations to the impedance vectors discussed in this letter. The conversion between these two representations is elucidated in [13, Eq. (6)] and [12, Eq. (35)–(39)]. We can further decompose $\mathbf{Z}_{\text{SS}} = \mathbf{Z}_{\text{SS}}^{\text{self}} + \mathbf{Z}_{\text{SS}}^{\text{mutual}}$, where $\mathbf{Z}_{\text{SS}}^{\text{self}} \in \mathbb{C}^{N \times N}$ is a diagonal matrix representing the self impedances of the RIS elements, and $\mathbf{Z}_{\text{SS}}^{\text{mutual}}$ is a matrix containing only the off-diagonal entries which stand for the mutual impedances among each pair of RIS elements. Hence, the matrix $\mathbf{Z}_{\text{SS}}^{\text{mutual}}$ characterizes the mutual coupling among RIS elements.

According to [8], the mutual impedances $\{\mathbf{z}_{\text{ST}}, \mathbf{z}_{\text{RS}}, \mathbf{Z}_{\text{SS}}\}$ depend only on the physical configuration of the radiators. When it is assumed that all radiators, including antennas and scatterers, are cylindrical thin wires of perfectly conducting material, the mutual impedances can be calculated explicitly [14]. For two cylindrical thin radiators (each with radius r) located at $\mathbf{p}_p = [x_p, y_p, z_p]^\top$ and $\mathbf{p}_q = [x_q, y_q, z_q]^\top$, the mutual impedance can be evaluated numerically by (2) given below [8], [14]. Here, $\eta_0 = \sqrt{\mu_0/\epsilon_0}$ and $k_0 = 2\pi/\lambda$ are the intrinsic impedance of free space and the wavenumber, where μ_0 , ϵ_0 , and λ denote the magnetic permeability, the electric permittivity, and the signal wavelength, respectively. The integral limit variables h_p and h_q represent the half-length of the two radiators and the function $R(\xi, z)$ accounting for the distance between \mathbf{p}_p and \mathbf{p}_q is given by

$$R(\xi, z) = \sqrt{\rho_1^2 + (z - \xi + \rho_2)^2}, \quad (3)$$

$$\begin{cases} \rho_1 = \sqrt{(x_p - x_q)^2 + (y_p - y_q)^2}, & \rho_2 = z_p - z_q, & \text{if } p \neq q, \\ \rho_1 = r, & \rho_2 = 0, & \text{if } p = q, \end{cases}$$

Here $p = q$ corresponds to the self-impedance case. Note that a shorter distance between \mathbf{p}_p and \mathbf{p}_q generates a lower value of $R(\xi, z)$, thus resulting in a higher mutual impedance according to (2). Fig. 2 plots a typical example of mutual coupling $|Z_{qp}|$ versus the inter-distance of two radiators.

B. Signal Model

In this work, we consider a scenario of an uplink transmission from an unknown user to a fixed base station through a fixed RIS. Suppose the transmitter sends a deterministic pilot signal $\sqrt{P_T} \cdot 1$, with power P_T , to the receiver via RIS. The received signal can be expressed as

$$y = \sqrt{P_T} \mathbf{z}_{\text{RS}}^\top (\mathbf{Z}_{\text{SS}} + \mathbf{Z}_{\text{RIS}})^{-1} \mathbf{z}_{\text{ST}} + \omega, \quad (4)$$

where $\omega \sim \mathcal{CN}(0, \sigma^2)$ models the thermal noise at the receiver. Since the locations of the receiver and RIS are known, the RIS-receiver channel \mathbf{z}_{RS} is assumed to be known. Hence,

the channel estimation problem in this paper focuses on the estimation of the unknown channel \mathbf{z}_{ST} .

The signal model (4) indicates that the observable y is a projection of \mathbf{z}_{ST} onto the direction of the vector $\sqrt{P_T} \mathbf{z}_{\text{RS}}^\top (\mathbf{Z}_{\text{SS}} + \mathbf{Z}_{\text{RIS}})^{-1}$ which depends on the RIS configuration \mathbf{Z}_{RIS} in addition to the mutual coupling \mathbf{Z}_{SS} . To estimate the unknown channel \mathbf{z}_{ST} , multiple transmissions are required and the RIS needs to switch between different configurations so that the projections of \mathbf{z}_{ST} in different directions are observable [15]. Suppose G transmissions are implemented at different time instants, during which the channel \mathbf{z}_{ST} stays constant and the RIS configuration is changed over these instances as $\mathbf{Z}_{\text{RIS},1}, \mathbf{Z}_{\text{RIS},2}, \dots, \mathbf{Z}_{\text{RIS},G}$. Then the total received signal can be concatenated as $\mathbf{y} = [y_1, \dots, y_G]^\top \in \mathbb{C}^{G \times 1}$, where $y_g = \sqrt{P_T} \mathbf{z}_{\text{RS}}^\top (\mathbf{Z}_{\text{SS}} + \mathbf{Z}_{\text{RIS},g})^{-1} \mathbf{z}_{\text{ST}} + \omega$, $g = 1, \dots, G$.

C. Problem Formulation and Analysis Objective

1) *The Channel Estimation Problem:* The goal of this letter is to analyze the impact of mutual coupling on the channel estimation of RIS-aided communication. Hence, we first clarify the considered mismatched channel estimation problem. To begin with, we define

$$\mathbf{B}(\mathbf{Z}_{\text{SS}}^{\text{self}}, \mathbf{Z}_{\text{SS}}^{\text{mutual}}) \triangleq \begin{bmatrix} \mathbf{z}_{\text{RS}}^\top (\mathbf{Z}_{\text{SS}}^{\text{self}} + \mathbf{Z}_{\text{SS}}^{\text{mutual}} + \mathbf{Z}_{\text{RIS},1})^{-1} \\ \vdots \\ \mathbf{z}_{\text{RS}}^\top (\mathbf{Z}_{\text{SS}}^{\text{self}} + \mathbf{Z}_{\text{SS}}^{\text{mutual}} + \mathbf{Z}_{\text{RIS},G})^{-1} \end{bmatrix}.$$

Then, the observations, i.e., the received signal with RIS mutual coupling, can be written as

$$\mathbf{y} = \sqrt{P_T} \mathbf{B}(\mathbf{Z}_{\text{SS}}^{\text{self}}, \mathbf{Z}_{\text{SS}}^{\text{mutual}}) \mathbf{z}_{\text{ST}} + \boldsymbol{\omega}, \quad (5)$$

where $\boldsymbol{\omega} \sim \mathcal{CN}(\mathbf{0}, \sigma^2 \mathbf{I}_G)$. Next, we consider a channel estimation problem using the mutual coupling-unaware model given by [9]

$$\mathbf{y} = \sqrt{P_T} \mathbf{B}(\mathbf{Z}_{\text{SS}}^{\text{self}}, \mathbf{0}) \mathbf{z}_{\text{ST}} + \boldsymbol{\omega}. \quad (6)$$

The considered channel estimation refers to estimating \mathbf{z}_{ST} based on the received signal \mathbf{y} , where \mathbf{y} is given by the true model (5) while the estimation is based on model (6) that does not account for mutual coupling.

2) *The Analysis Objective:* Since we neglect the mutual coupling, the estimation model (6) is mismatched with the true model (5). Thus, our analyses aim to offer insights into how this mismatch affects the estimation performance.

We further express these quantities in terms of the real and imaginary components as

$$\mathbf{D}(\mathbf{Z}_{\text{SS}}^{\text{self}}, \mathbf{Z}_{\text{SS}}^{\text{mutual}}) = \begin{bmatrix} \text{Re}(\mathbf{B}) & -\text{Im}(\mathbf{B}) \\ \text{Im}(\mathbf{B}) & \text{Re}(\mathbf{B}) \end{bmatrix} \in \mathbb{R}^{2G \times 2N}, \quad (7)$$

$$\mathbf{r} = [\text{Re}(\mathbf{y}^\top), \text{Im}(\mathbf{y}^\top)]^\top, \quad \mathbf{x} = [\text{Re}(\mathbf{z}_{\text{ST}}^\top), \text{Im}(\mathbf{z}_{\text{ST}}^\top)]^\top, \quad (8)$$

$$Z_{qp} = \frac{j\eta_0}{4\pi k_0} \int_{-h_q}^{h_q} \int_{-h_p}^{h_p} \frac{e^{-jk_0 R(\xi, z)} \sin(k_0(h_p - |\xi|)) \sin(k_0(h_q - |z|))}{R(\xi, z) \sin(k_0 h_p) \sin(k_0 h_q)} \left(k_0^2 - \frac{jk_0}{R(\xi, z)} - \frac{k_0^2(z - \xi + \rho_2)^2 + 1}{R^2(\xi, z)} + \frac{3jk_0(z - \xi + \rho_2)^2}{R^3(\xi, z)} + \frac{3(z - \xi + \rho_2)^2}{R^4(\xi, z)} \right) d\xi dz, \quad (2)$$

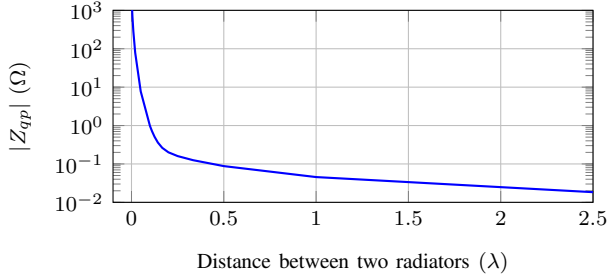


Fig. 2. An example of $|Z_{qp}|$ versus the inter-distance of two radiators with $h_p = h_q = \lambda/64$ and $r = \lambda/500$ at frequency of 28 GHz.

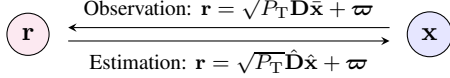


Fig. 3. Illustration of the mutual coupling-introduced model mismatch in the considered RIS-assisted channel estimation problem.

where $\text{Re}(\cdot)$ and $\text{Im}(\cdot)$ respectively return the real and imaginary parts of a complex vector or matrix. Thus, the observation model (5) and the estimation model (6) can be rewritten as

$$\text{Obs. model: } \mathbf{r} = \sqrt{P_T} \mathbf{D}(\mathbf{Z}_{SS}^{\text{self}}, \mathbf{Z}_{SS}^{\text{mutual}}) \mathbf{x} + \boldsymbol{\varpi} \in \mathbb{R}^{2G}, \quad (9)$$

$$\text{Est. model: } \mathbf{r} = \sqrt{P_T} \mathbf{D}(\mathbf{Z}_{SS}^{\text{self}}, \mathbf{0}) \mathbf{x} + \boldsymbol{\varpi} \in \mathbb{R}^{2G}, \quad (10)$$

where $\boldsymbol{\varpi} \sim \mathcal{N}(\mathbf{0}, \frac{\sigma^2}{2} \mathbf{I}_{2G})$. Hence, the channel estimation problem can be equally stated as recovering \mathbf{x} given \mathbf{r} .

For the sake of better illustration, we denote

$$\bar{\mathbf{D}} = \mathbf{D}(\mathbf{Z}_{SS}^{\text{self}}, \mathbf{Z}_{SS}^{\text{mutual}}), \quad \hat{\mathbf{D}} = \mathbf{D}(\mathbf{Z}_{SS}^{\text{self}}, \mathbf{0}). \quad (11)$$

In addition, we use $\bar{\mathbf{x}}$ and $\hat{\mathbf{x}}$ to represent the true unknown channel and the estimated channel through the mismatched model that ignores the RIS mutual coupling, respectively. Then the involved model mismatch can be illustrated as Fig. 3. We are interested in the behavior of the estimation root mean square error (RMSE) $\sqrt{\mathbb{E}\|\hat{\mathbf{x}} - \bar{\mathbf{x}}\|^2}$ under this model mismatch, which can be analyzed using the tool of MCRB.

III. MCRB ANALYSIS

The MCRB is a generalization of the well-known Cramér-Rao lower bound (CRLB) to the cases with a model mismatch, which gives a lower bound for the estimation RMSE [11], [16]. Based on Fig. 3, we have the true likelihood function f_T and the mismatched likelihood function f_M as

$$f_T(\mathbf{r}; \mathbf{x}) = \frac{1}{(\pi\sigma^2)^G} e^{-\frac{\|\mathbf{r} - \sqrt{P_T} \bar{\mathbf{D}} \mathbf{x}\|^2}{\sigma^2}}, \quad (12)$$

$$f_M(\mathbf{r}; \mathbf{x}) = \frac{1}{(\pi\sigma^2)^G} e^{-\frac{\|\mathbf{r} - \sqrt{P_T} \hat{\mathbf{D}} \mathbf{x}\|^2}{\sigma^2}}. \quad (13)$$

Based on model f_M , the lower bound matrix of the estimation mean square error (MSE) can be obtained as [11]

$$\text{LBM}(\hat{\mathbf{x}}, \bar{\mathbf{x}}) = \underbrace{\mathbf{A}_{\mathbf{x}_0}^{-1} \mathbf{B}_{\mathbf{x}_0} \mathbf{A}_{\mathbf{x}_0}^{-1}}_{\text{MCRB}(\mathbf{x}_0)} + \underbrace{(\bar{\mathbf{x}} - \mathbf{x}_0)(\bar{\mathbf{x}} - \mathbf{x}_0)^T}_{\text{Bias}(\mathbf{x}_0)}, \quad (14)$$

thus the RMSE of the channel estimation under model mismatch is lower bounded as

$$\sqrt{\mathbb{E}\|\hat{\mathbf{x}} - \bar{\mathbf{x}}\|^2} \geq \sqrt{\text{Tr}(\text{LBM}(\hat{\mathbf{x}}, \bar{\mathbf{x}}))} \triangleq \text{LB}, \quad (15)$$

where $\text{Tr}(\cdot)$ returns the trace of a matrix. Here, \mathbf{x}_0 is the pseudo-true parameter vector that minimizes the Kullback-Leibler divergence (KLD) between f_T and f_M , i.e.,

$$\mathbf{x}_0 = \arg \min_{\mathbf{x}} \text{KLD}(f_T(\mathbf{r}; \bar{\mathbf{x}}) \| f_M(\mathbf{r}; \mathbf{x})), \quad (16)$$

and matrices $\mathbf{A}_{\mathbf{x}_0}$ and $\mathbf{B}_{\mathbf{x}_0}$ are defined as

$$\mathbf{A}_{\mathbf{x}_0} = \mathbb{E}_{f_T} \left\{ \frac{\partial^2}{\partial \mathbf{x}^2} \ln f_M(\mathbf{r}; \mathbf{x}) \Big|_{\mathbf{x}=\mathbf{x}_0} \right\}, \quad (17)$$

$$\mathbf{B}_{\mathbf{x}_0} = \mathbb{E}_{f_T} \left\{ \frac{\partial \ln f_M(\mathbf{r}; \mathbf{x})}{\partial \mathbf{x}} \left(\frac{\partial \ln f_M(\mathbf{r}; \mathbf{x})}{\partial \mathbf{x}} \right)^T \Big|_{\mathbf{x}=\mathbf{x}_0} \right\}. \quad (18)$$

A. MCRB Derivation

Now we focus on evaluating \mathbf{x}_0 , $\mathbf{A}_{\mathbf{x}_0}$, and $\mathbf{B}_{\mathbf{x}_0}$ that appear in (14). According to the definition of KLD [17], we can write

$$\begin{aligned} \text{KLD}(f_T(\mathbf{r}; \bar{\mathbf{x}}) \| f_M(\mathbf{r}; \mathbf{x})) &= \mathbb{E}_{f_T} \{ \ln f_T(\mathbf{r}; \bar{\mathbf{x}}) - \ln f_M(\mathbf{r}; \mathbf{x}) \}, \\ &= \frac{1}{\sigma^2} \mathbb{E}_{f_T} \left\{ \|\mathbf{r} - \sqrt{P_T} \bar{\mathbf{D}} \bar{\mathbf{x}}\|^2 \right\} + \frac{1}{\sigma^2} \mathbb{E}_{f_T} \left\{ \|\mathbf{r} - \sqrt{P_T} \hat{\mathbf{D}} \mathbf{x}\|^2 \right\}, \\ &= \frac{P_T}{\sigma^2} \|\bar{\mathbf{D}} \bar{\mathbf{x}} - \hat{\mathbf{D}} \mathbf{x}\|^2. \end{aligned} \quad (19)$$

It thus follows that

$$\mathbf{x}_0 = \arg \min_{\mathbf{x}} \|\bar{\mathbf{D}} \bar{\mathbf{x}} - \hat{\mathbf{D}} \mathbf{x}\|^2 = (\hat{\mathbf{D}}^T \hat{\mathbf{D}})^{-1} \hat{\mathbf{D}}^T \bar{\mathbf{D}} \bar{\mathbf{x}}. \quad (20)$$

Substituting f_M from (13) in (17) and (18) yields

$$\mathbf{A}_{\mathbf{x}_0} = -\mathbf{B}_{\mathbf{x}_0} = -\frac{2P_T}{\sigma^2} \hat{\mathbf{D}}^T \hat{\mathbf{D}}. \quad (21)$$

By substituting (20) and (21) into (14), we finally obtain

$$\text{LBM}(\hat{\mathbf{x}}, \bar{\mathbf{x}}) = \underbrace{\frac{1}{2\gamma} (\hat{\mathbf{D}}^T \hat{\mathbf{D}})^{-1}}_{\text{MCRB}(\mathbf{x}_0)} + \underbrace{(\bar{\mathbf{x}} - \Phi \bar{\mathbf{x}})(\bar{\mathbf{x}} - \Phi \bar{\mathbf{x}})^T}_{\text{Bias}(\mathbf{x}_0)}, \quad (22)$$

where $\Phi = (\hat{\mathbf{D}}^T \hat{\mathbf{D}})^{-1} \hat{\mathbf{D}}^T \bar{\mathbf{D}}$ and $\gamma \triangleq P_T/\sigma^2$ is the signal-to-noise ratio (SNR).

B. Results Analysis

Fig. 4 provides an intuitive illustration of (14) and (15). Under a certain model mismatch, the estimates (e.g., using a maximum likelihood estimator) converge to the pseudo-true parameters as the SNR increases [11]. As shown in Fig. 4, the MCRB term in (14) lower bounds the MSE between the estimates $\hat{\mathbf{x}}$ and the pseudo-true parameter \mathbf{x}_0 , while the Bias term accounts for the distance between pseudo-true parameter \mathbf{x}_0 and the true unknown parameter $\bar{\mathbf{x}}$. Based on the results in (22), the following insights are further gained.

Remark 1: The MCRB term in (22) decreases with increasing SNR and finally converges to zero. The value of MCRB at a certain SNR depends only on the mismatched model $\hat{\mathbf{D}}$ itself, and is independent of the true model $\bar{\mathbf{D}}$ and the divergence between the true and mismatched models.

Remark 2: The Bias term in (22) is independent of SNR. Instead, it depends only on the mismatch between $\bar{\mathbf{D}}$ and $\hat{\mathbf{D}}$.

Remark 3: In the low SNR region where MCRB is dominant, LB can be approximated by $\sqrt{\text{Tr}(\text{MCRB})}$; While in the high SNR region where MCRB converges to zero, LB will saturate to $\sqrt{\text{Tr}(\text{Bias})}$, as demonstrated in Fig. 4.

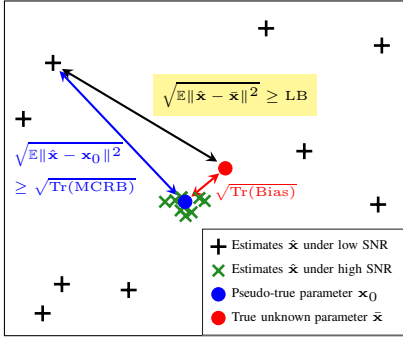


Fig. 4. Illustration of the relationship between MCRB, Bias, and LB.

Remark 4: When we estimate using the true model, i.e., $\hat{\mathbf{D}} = \bar{\mathbf{D}}$, the mismatched LB is reduced to the classical CRLB, which is obtained as $\text{CRLB} = \sqrt{\text{Tr}(\text{MCRB})} = \sqrt{\frac{1}{2\gamma} \text{Tr}\{\bar{\mathbf{D}}^T \bar{\mathbf{D}}\}}$ from (22). Remarkably, according to *Remark 1*, we can infer that the estimation MSE using the correct model does not necessarily outperform the mismatched model in the MCRB-dominant regions, since the MCRB term depends only on the used model itself.

IV. NUMERICAL RESULTS

This section reports numerical results. The simulations setups are as follows: $h_p = h_q = \lambda/64$, $r = \lambda/500$, the signal frequency $f = 28$ GHz, the position of the transmitter is (5 m, -5 m, 3 m), the position of the receiver is (5 m, 5 m, 1 m), and the RIS is centered at (0 m, 0 m, 0 m), which are the same as [8]. In addition, the number of transmissions $G = 256$. For the g th transmission, we set the tunable load of the n th RIS element as $Z_{\text{RIS},n,g} = R_{\text{RIS},n,g} + j\omega L_{\text{RIS},n,g}$, where $\omega = 2\pi f$, $R_{\text{RIS},n,g}$ is randomly generated from $[0.1 \Omega, 10.1 \Omega]$, and $L_{\text{RIS},n,g}$ is randomly generated from $[0.1 \text{ nH}, 10.1 \text{ nH}]$. By default, the RIS size is 4×4 , the noise PSD is -173.855 dBm/Hz, and the noise figure is 10 dB.

A. Impact of Ignoring Mutual Coupling

This subsection evaluates the impact of ignoring mutual coupling on RIS-assisted channel estimation. We first study the behavior of the derived bounds at different SNR levels. To verify our bound derivation, we test the RMSEs of the maximum likelihood (ML) estimator $\hat{\mathbf{x}} = \frac{1}{\sqrt{P_T}} (\hat{\mathbf{D}}^T \hat{\mathbf{D}})^{-1} \hat{\mathbf{D}}^T \mathbf{r}$ and compare them with the derived bounds. The observation \mathbf{r} is generated based on the true model $\bar{\mathbf{D}}$. As clarified in Section II-A, mutual coupling relies on RIS element spacing d , which affects the mutual impedance matrix $\mathbf{Z}_{\text{SS}}^{\text{mutual}}$ and in turn varies the true model $\bar{\mathbf{D}}$ according to (7). For the sake of clarity, we use $\bar{\mathbf{D}}(d) = \mathbf{D}(\mathbf{Z}_{\text{SS}}^{\text{self}}, \mathbf{Z}_{\text{SS}}^{\text{mutual}}(d))$ to indicate that $\bar{\mathbf{D}}$ is a function of d . In contrast, $\hat{\mathbf{D}}$ is unrelated to d since it ignores the mutual coupling effect as shown in (11).

Fig. 5 presents the comparison of the derived LB and the tested RMSE of the ML estimator. We use $\text{LB}(\bar{\mathbf{D}}(d), \hat{\mathbf{D}})$ to denote the case that generates observations using $\bar{\mathbf{D}}(d)$ and estimates using $\hat{\mathbf{D}}$, and the corresponding RMSE is denoted as $\text{RMSE}(\bar{\mathbf{D}}(d), \hat{\mathbf{D}})$. The classical CRLB which corresponds

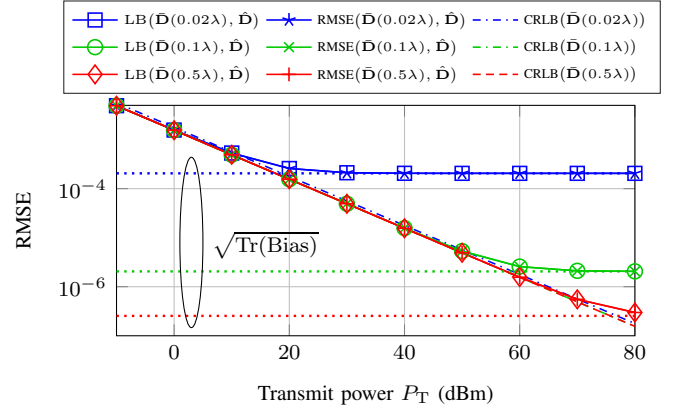


Fig. 5. Comparison of the derived lower bounds and the RMSE of the ML estimator versus transmit power (SNR).

to the case $\hat{\mathbf{D}} = \bar{\mathbf{D}}(d)$ is also plotted in Fig. 5 and denoted as $\text{CRLB}(\bar{\mathbf{D}}(d))$. In Fig. 5, the RMSEs of the ML estimator closely follows the derived LBs, demonstrating the validity of our derivation. The LBs decreases with the increase of P_T at low-power regions (MCRB dominates) but finally saturates as P_T increases (Bias dominates), which is consistent with the analysis in *Remark 3*. Moreover, we notice that a shorter d generates a higher $\sqrt{\text{Tr}(\text{Bias})}$, which indicates a greater performance degradation. For example, when $d = 0.02\lambda$, the performance starts to saturate at around $P_T = 10$ dBm, which implies that ignoring mutual coupling degrades the channel estimation performance for the regions $P_T > 10$ dBm; Nonetheless, the mismatch of the case $d = 0.5\lambda$ does not cause a performance saturation until around $P_T = 70$ dBm, which indicates that we can safely ignore the mutual coupling effect in the scenarios $P_T < 70$ dBm for the setup $d = 0.5\lambda$.

The above results reveal that the mismatch bias $\sqrt{\text{Tr}(\text{Bias})}$ is a direct metric evaluating the impact of ignoring mutual coupling on channel estimation, since it represents the best performance that can be achieved over all the SNRs. On the other hand, a lower value of $\sqrt{\text{Tr}(\text{Bias})}$ means it is safe to ignore the mutual coupling effect at a wider region of SNR. To manifestly show the impact of ignoring mutual coupling over different RIS element spacing, Fig. 6 presents the evaluation of $\sqrt{\text{Tr}(\text{Bias})}$ versus d . In this trial, we test 3 different RIS sizes as $\{4 \times 4, 8 \times 8, 12 \times 12\}$. The results show that the bias term for all the tested RIS sizes increases as the RIS element spacing shortens and finally keeps flat at the region $d < 0.02\lambda$. This concludes that the shorter the RIS element spacing, the greater the impact on the considered channel estimation problem until $d < 0.02\lambda$ where the impact keeps flat. Additionally, it is observed that with a fixed RIS element spacing, the larger the size of RIS, the greater the impact of ignoring mutual coupling.

B. Evaluation of Mutual Coupling-Aware Estimation

Now we evaluate the impact of the mutual coupling effect in the mutual coupling-aware channel estimation. Suppose the estimator has the information of $\mathbf{Z}_{\text{SS}}^{\text{mutual}}$, i.e., $\hat{\mathbf{D}} = \bar{\mathbf{D}}$, thus the estimation RMSE is lower bounded by the classical CRLB, as clarified in *Remark 4*. Fig. 7 shows the evaluation of the mismatch-free CRLB versus RIS element spacing d

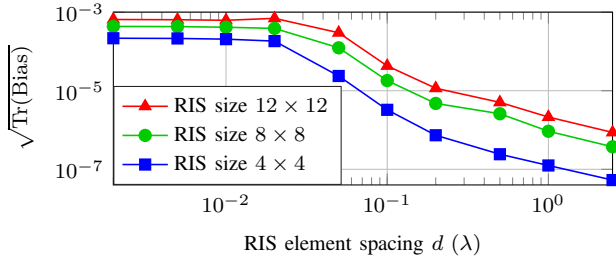


Fig. 6. Evaluation of $\sqrt{\text{Tr}(\text{Bias})}$ versus RIS element spacing d for different RIS size of $\{4 \times 4, 8 \times 8, 12 \times 12\}$.

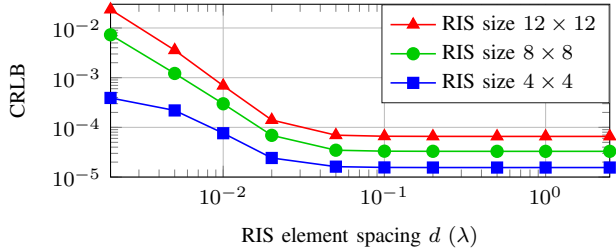


Fig. 7. Evaluation of the mismatch-free CRLB versus RIS element spacing d for different RIS size of $\{4 \times 4, 8 \times 8, 12 \times 12\}$ with $P_T = 40$ dBm.

for different RIS size of $\{4 \times 4, 8 \times 8, 12 \times 12\}$, where the transmit power is fixed as $P_T = 40$ dBm. It unveils that at the large-spacing regions ($d > 0.05 \lambda$), mutual coupling does not affect the performance bounds in a mutual coupling-aware estimation. However, when the RIS element spacing $d < 0.05 \lambda$, the CRLBs increase with the decrease of d . This shows that even with the mismatch-free setup (i.e., the mutual impedance $\mathbf{Z}_{SS}^{\text{mutual}}$ is known), the mutual coupling effect can degrade the channel estimation performance if the RIS element spacing is too small ($d < 0.05 \lambda$). Finally, we have the observation that for a fixed d , the larger the size of RIS, the higher the CRLB. This is because a larger RIS size increases the dimension of the unknown channel vector, making channel estimation more challenging.

Lessons Learned: As the densification of RIS unit cells amplifies the impact of mutual coupling, particularly in applications like holographic MIMO [10], disregarding this effect becomes untenable. By carefully adjusting the RIS configuration, it is possible to mitigate the influence of mutual coupling, as demonstrated in [9], thereby enhancing channel estimation performance. Nevertheless, such an optimization over RIS configuration necessitates knowledge of mutual impedance among RIS unit cells, which can be obtained through a calibration process, either online or offline. Practically, the RIS configuration and channel estimation can be performed alternately, which may augment pilot transmission, indicating a trade-off between pilot overhead and estimation performance.

V. CONCLUSION

This study examined the impact of mutual coupling on channel estimation within a RIS-assisted communication system. Specifically, we derived the MCRB of RIS-assisted channel estimation, which accounts for the model mismatch caused by the neglect of mutual coupling. Our analysis and numerical results reveal that ignoring mutual coupling in scenarios involving closer integration of RIS elements or larger RIS size

leads to a more pronounced degradation in channel estimation performance. Conversely, even with mutual coupling-aware setups, too tight RIS element spacing can also lead to significant estimation performance degradation. Future work can focus on the development of mutual coupling-aware channel estimation algorithms, antenna array design, and improvement of the computing ability of metasurfaces.

REFERENCES

- [1] E. Björnson, H. Wymeersch, B. Matthiesen, P. Popovski, L. Sanguinetti, and E. de Carvalho, "Reconfigurable intelligent surfaces: A signal processing perspective with wireless applications," *IEEE Signal Processing Magazine*, vol. 39, no. 2, pp. 135–158, 2022.
- [2] H. Sarieddeen, M.-S. Alouini, and T. Y. Al-Naffouri, "An overview of signal processing techniques for terahertz communications," *Proceedings of the IEEE*, vol. 109, no. 10, pp. 1628–1665, 2021.
- [3] P. Zheng, H. Chen, T. Ballal, M. Valkama, H. Wymeersch, and T. Y. Al-Naffouri, "JrCUP: Joint RIS calibration and user positioning for 6G wireless systems," *IEEE Transactions on Wireless Communications (early access)*, 2023.
- [4] H. Chen, P. Zheng, M. F. Keskin, T. Al-Naffouri, and H. Wymeersch, "Multi-RIS-enabled 3D sidelink positioning," *IEEE Transactions on Wireless Communications (early access)*, 2023.
- [5] E. Björnson, Ö. Özdogan, and E. G. Larsson, "Intelligent reflecting surface versus decode-and-forward: How large surfaces are needed to beat relaying?" *IEEE Wireless Communications Letters*, vol. 9, no. 2, pp. 244–248, 2020.
- [6] J. He, H. Wymeersch, and M. Juntti, "Channel estimation for RIS-aided mmWave MIMO systems via atomic norm minimization," *IEEE Transactions on Wireless Communications*, vol. 20, no. 9, pp. 5786–5797, 2021.
- [7] J. An, C. Xu, L. Gan, and L. Hanzo, "Low-complexity channel estimation and passive beamforming for RIS-assisted MIMO systems relying on discrete phase shifts," *IEEE Transactions on Communications*, vol. 70, no. 2, pp. 1245–1260, 2022.
- [8] G. Gradoni and M. Di Renzo, "End-to-end mutual coupling aware communication model for reconfigurable intelligent surfaces: An electromagnetic-compliant approach based on mutual impedances," *IEEE Wireless Communications Letters*, vol. 10, no. 5, pp. 938–942, 2021.
- [9] X. Qian and M. D. Renzo, "Mutual coupling and unit cell aware optimization for reconfigurable intelligent surfaces," *IEEE Wireless Communications Letters*, vol. 10, no. 6, pp. 1183–1187, 2021.
- [10] J. An, C. Yuen, C. Huang, M. Debbah, H. V. Poor, and L. Hanzo, "A tutorial on holographic MIMO communications—Part III: Open opportunities and challenges," *IEEE Communications Letters*, vol. 27, no. 7, pp. 1674–1678, 2023.
- [11] S. Fortunati, F. Gini, M. S. Greco, and C. D. Richmond, "Performance bounds for parameter estimation under misspecified models: Fundamental findings and applications," *IEEE Signal Processing Magazine*, vol. 34, no. 6, pp. 142–157, 2017.
- [12] S. Shen, B. Clerckx, and R. Murch, "Modeling and architecture design of reconfigurable intelligent surfaces using scattering parameter network analysis," *IEEE Transactions on Wireless Communications*, vol. 21, no. 2, pp. 1229–1243, 2022.
- [13] H. Li, S. Shen, M. Nerini, M. Di Renzo, and B. Clerckx, "Beyond diagonal reconfigurable intelligent surfaces with mutual coupling: Modeling and optimization," *arXiv preprint arXiv:2310.02708*, 2023.
- [14] M. Di Renzo, V. Galdi, and G. Castaldi, "Modeling the mutual coupling of reconfigurable metasurfaces," in *17th European Conference on Antennas and Propagation (EuCAP)*, 2023.
- [15] E. Björnson and P. Ramezani, "Maximum likelihood channel estimation for RIS-aided communications with LOS channels," in *56th Asilomar Conference on Signals, Systems, and Computers*, 2022, pp. 403–407.
- [16] P. Zheng, H. Chen, T. Ballal, H. Wymeersch, and T. Y. Al-Naffouri, "Misspecified Cramér-Rao bound of RIS-aided localization under geometry mismatch," in *IEEE International Conference on Acoustics, Speech and Signal Processing (ICASSP)*, 2023.
- [17] A. H. Sayed, *Inference and Learning from Data: Inference*. Cambridge University Press, 2022, vol. 2.